



Cite this: *Nanoscale*, 2022, **14**, 5701

# Synthesis of silver and gold nanoparticles–enzyme–polymer conjugate hybrids as dual-activity catalysts for chemoenzymatic cascade reactions†

Janne M. Naapuri,<sup>a,b,c</sup> Noelia Losada-Garcia,<sup>a</sup> Jan Deska<sup>a</sup> and Jose M. Palomo<sup>a</sup>

Novel hybrids containing silver or gold nanoparticles have been synthesized in aqueous media and at room temperature using enzymes or tailor-made enzyme–polymer conjugates, which directly induced the formation of inorganic silver or gold species. The choice of pH, protein, or bioconjugate strongly affected the final metallic nanoparticles hybrid formation. Using *Candida antarctica* lipase (CALB) in a solution, nanobiohybrids containing Ag<sub>2</sub>O nanoparticles of 9 nm average diameter were obtained. The use of tailor-made bioconjugates, for example, the CALB modified with dextran-aspartic acid polymer (Dext6kDa), resulted in a nanobiohybrid containing smaller Ag(0)/Ag<sub>2</sub>O nanoparticles. In the case of nanobiohybrids based on gold, Au(0) species were found in all cases. The Au–CALB hybrid contained spherical nanoparticles with 18 nm average diameter size, with a minor range of larger ones (>100 nm) while the AuNPs–CALB–Dext6kDa hybrid was formed by much smaller nanoparticles (9 nm, minor range of 22 nm), and also nanorods of 20–30/40–50 nm length. Using *Thermomyces lanuginosus* lipase (TLL), apart from the nanoparticle formation, nanoflowers with a diameter range of 100–200 nm were obtained. All nanobiohybrids maintained (dual) enzymatic and metallic activities. For instance, these nanobiohybrids exhibited exquisite dual-activity for hydrolysis/cycloisomerization cascades starting from allenic acetates. By merging the transition metal reactivity with the inherent lipase catalysis, allenic acetates directly converted to the corresponding O-heterocycles in enantiopure form catalysed by AgNPs–CALB–Dext6kDa, taking advantage of a kinetic resolution/cyclization pathway. These results showed the high applicability of these novel hybrids, offering new opportunities for the design of novel reaction cascades.

Received 19th January 2022,  
Accepted 14th March 2022

DOI: [10.1039/d2nr00361a](https://doi.org/10.1039/d2nr00361a)

[rsc.li/nanoscale](http://rsc.li/nanoscale)

## Introduction

Catalysis with silver and gold has gained momentum over the past years and found extended application in organic chemistry.<sup>1,2</sup> Although these metals are less extensively used as catalysts than palladium, specific application of Ag(I) as soft Lewis acid or Au(0) through its anisotropic provide new opportunities in chemical processes.<sup>3–7</sup> In particular, the development of single and smaller nanoparticles of both metals as

efficient catalysts in different processes has been recently described as a new alternative.<sup>7–12</sup>

However, synthetic strategies to control the metal species and the size of these nanoparticles, key factors in the final catalytic efficiency, are essential.<sup>10,11</sup> In the literature, they are mainly based on the application of a reducing agent from a metal salt solution, which can be in an organic solvent or aqueous media. These methodologies allowed to create the nanoparticles but in many cases with large sizes. In the last few years, in our group, we have developed a novel methodology for metal nanoparticle hybrids, which is based on the application of a protein in the synthesis.<sup>12–17</sup> This approach consists of a very efficient and sustainable method, where, we have obtained well-defined small nanoparticles of several metals (Pd, Fe, Cu).<sup>12–17</sup> A catalytic protein (enzyme) is used as a scaffold, where it takes on several important roles: providing stabilization for nanoparticles, *in situ* formation of nano-

<sup>a</sup>Department of Biocatalysis, Institute of Catalysis (ICP-CSIC), Marie Curie 2, 28049 Madrid, Spain. E-mail: [josempalomo@icp.csic.es](mailto:josempalomo@icp.csic.es)

<sup>b</sup>Department of Chemistry, University of Helsinki, A. I. Virtasen aukio 1, 00560 Helsinki, Finland. E-mail: [jan.deska@helsinki.fi](mailto:jan.deska@helsinki.fi)

<sup>c</sup>Department of Chemistry, Aalto University, Kemistintie 1, 02150 Espoo, Finland

†Electronic supplementary information (ESI) available. See DOI: [10.1039/d2nr00361a](https://doi.org/10.1039/d2nr00361a)



particles (protein as a reducing agent), controlling the nanoparticle size and use as protein network for a final heterogeneous material. The crystalline metal nanoparticles are well dispersed in the protein network, avoiding the common problem of aggregation.

The mechanism of nanobiohybrid formation goes through three distinct steps (Fig. S1†), with the protein playing a key role in all of them. The formation is initiated by a metal ion binding event, followed by a reducing step. These two steps in the formation of nanobiohybrid can be explained considering the properties of amino acids or small peptides as it has been described in the literature. An ideal peptide sequence must present amino acids with moderate binding affinity for both the metal ions and the subsequently-formed metal particles (*i.e.*, amino acids presenting hydrophobic or charged side chains (with the opposite charge to that of the metal ions)) together with neighboring amino acids showing a strong reducing ability (*i.e.*, especially amino acids presenting hydrophobic side chains). Thus, keeping in mind the general rules described for tailor-made peptide synthesis and considering an enzyme as a complex structure of polypeptide chains. For example, the CALB amino acid sequence has been analyzed examining for some naturally present binding/reducing sequences.<sup>14</sup> Effectively, as shown in Fig. S1†, the enzyme surface contains many peptide sequences possessing the desired binding/reducing activities to adsorb metal ions. The metal ions then act as cross-linkers between the enzyme molecules, reducing their solubility and finally inducing the initial fast precipitation. Once brought closer to the hydrophobic reducing amino acids (for example, Trp (5), Tyr (9), Phe (10) are present in the CALB structure), the metal ions are reduced to their metallic state (Fig. S1†), also by the reductive ability of polyols (hydroxyl residues of Ser (31) and Thr (37) in the CALB structure). Finally, the growth of the nanoparticles is also con-

trolled by the constrained space within the protein matrix, generally resulting in small-size nanoparticles.

Here, the nanohybrid technology has been applied for the preparation of novel Ag and AuNPs–enzyme hybrids. These are two interesting examples of chemoenzymatic cascade processes. Other methods of synthesis of these metal nanoparticles have been tried by using biological molecules, although most of them with microorganisms or plant extracts and rarely with enzymes.<sup>14</sup> Recent studies have demonstrated that the physical or chemical modification of enzymes generates novel bioconjugates with improved catalytic properties.<sup>18–21</sup> This is a very important issue, in particular, when a cascade process is developed. These novel nanobiohybrids could have a pivotal advantage over other systems since they are able to exhibit an enzymatic and metallic activity in the same compartment. We recently demonstrated this unique property in the successful application of cascade processes.<sup>22,23</sup> Consequently, the preparation of novel hybrids using bioconjugates enzymes as matrix represents an appealing goal to widen the applicability of this new alternative strategy. Among the different cascade designs, asymmetric and stereoselective processes represent one of the most interesting ones presently, for example in the industrial synthesis of pharmaceutical products.<sup>24–26</sup>

Allenes have emerged as versatile precursors for the syntheses of heterocyclic compounds,<sup>27–29</sup> and the final products are important building blocks in the synthesis of valuable bioactive compounds.<sup>30–32</sup> In this way, pure enantiomers of dihydrofurans can be produced by combining metal-catalyzed allenic alcohol cycloisomerizations with lipase-induced kinetic resolution hydrolysis of allenic acetates.<sup>33</sup> Here, we evaluated novel silver and gold nanobiohybrids as dual-activity catalysts in the cascade synthesis of dihydrofurans, achieving excellent conversions and enantioselectivities (Fig. 1).

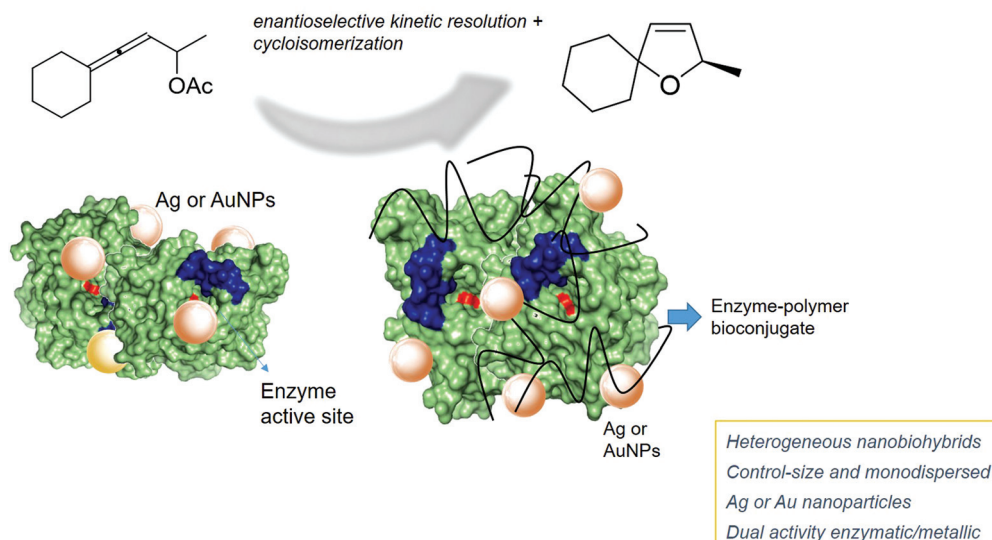


Fig. 1 Novel Ag and Au nanobiohybrids as dual catalysts for stereoselective cyclization reactions proposed in this work.



## Results and discussion

### Synthesis and characterization of Ag nanoparticles–enzyme hybrids

The preparation of Ag nanobiohybrids was attempted by employing an enzyme solution in aqueous media and using silver nitrate (Fig. 2a and Fig. S2†). First, lipase from *Candida antarctica* (fraction B) was directly dissolved in distilled water ( $\text{pH} \cong 6$ ) to a final concentration of  $0.3 \text{ mg mL}^{-1}$ . The  $\text{Ag}^+$  salt was added in the solid form directly to each protein solution. Considering our previous observations in the formation of palladium nanoparticles induced by this hydrolase,<sup>12,23</sup> a cloudy solution has proven to be indicative of the incipient formation of the hybrid between the enzyme and the metals is promising for the final generation of nanoparticles without the need of adding a reducing agent. A precipitate was rapidly formed and after 24 h of incubation, a clear solid material was obtained. By evaluating the amount of silver salt added, a  $20 \text{ mg mL}^{-1}$

concentration proved optimal for the solid formation. The pH of the solution was monitored during and at the final point of the synthesis and no significant changes were observed. Characterization of the obtained solid by X-ray diffraction (XRD) analysis revealed the formation of  $\text{Ag}_2\text{O}$  as unique silver species in both cases (matched well with JCPDS No. 00-076-1393) (Fig. 2b). SEM analysis demonstrated the formation of a heterogeneous aggregate (Fig. 2c). The nanoparticle formation within the enzyme network was confirmed by transmission electron microscopy (TEM) analysis. Silver nanoparticles with an average diameter size of around 9 nm, with a minor fraction with sizes  $>20 \text{ nm}$ , were thus obtained (Fig. 2d and e). These nanoparticles were synthesized directly by the enzyme, which acts as *in situ* reducing agent. The ICP-OES analysis confirmed the presence of about 25% content of silver.

Recently we have demonstrated that proteins bioconjugation, for example, with peptides, can have an influence on the metallic nanoparticle formation in the final nanohybrid.<sup>34</sup>

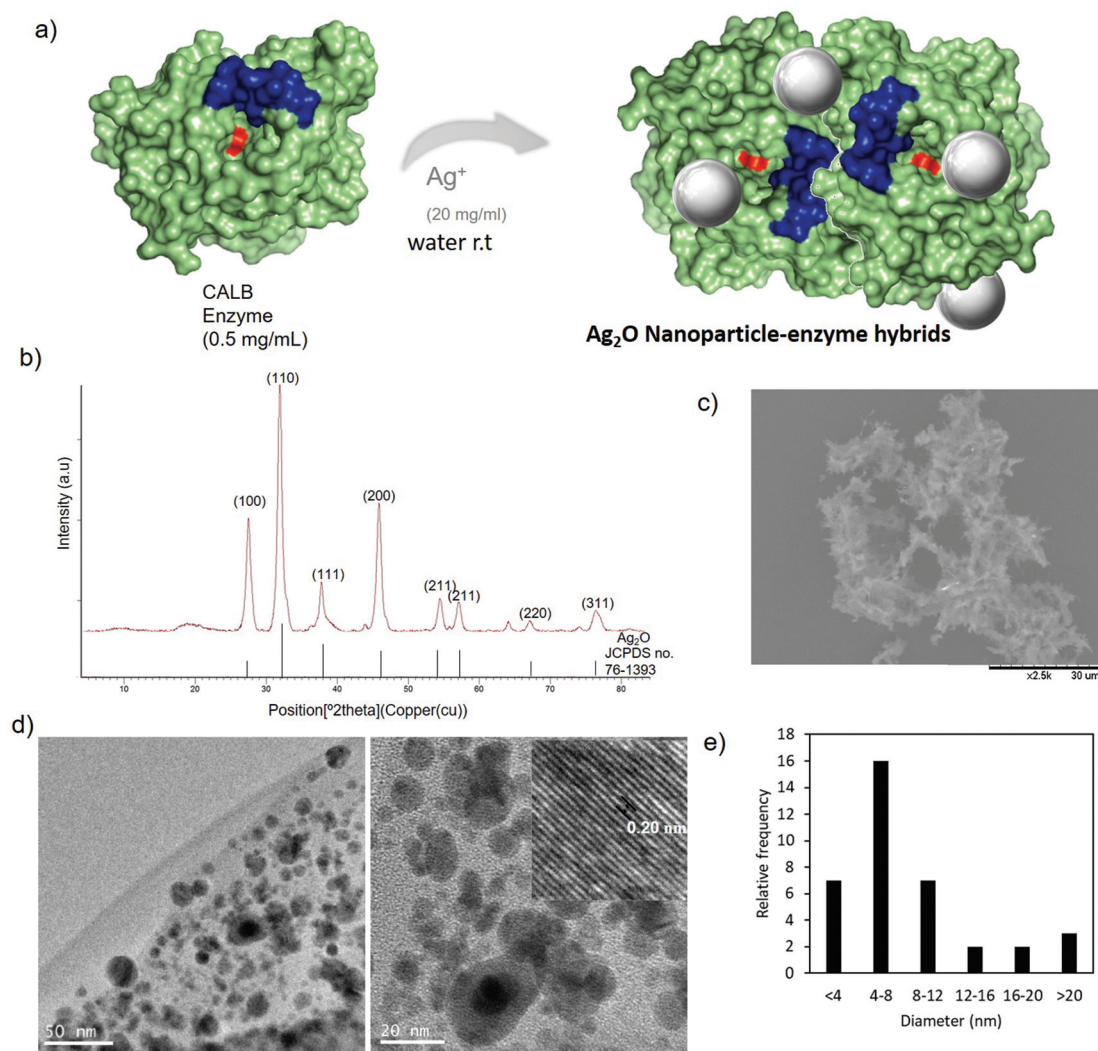


Fig. 2 Synthesis of AgNPs–CALB. (a) Synthetic scheme. (b) XRD pattern. (c) SEM image. (d) TEM images (inset IFFT). (e) Particle size distribution.





One of the simplest strategies to create protein bioconjugates, however, has been the coating with ionic polymers, which are important, for example, for the stability or activity of the enzymes.<sup>19</sup> In this term, and focus on the final application in a cascade system where dual (metallic and enzymatic) activities are crucial for success, two different sets of enzyme–protein conjugates were prepared and used for the fabrication of Ag nanobiohybrids (Fig. 3). On one side, CALB was coated by cation exchange with polyethyleneimine (PEI), an amino-functionalized hydrophilic polymer available in two different molecular weights (800 Da and 750 kDa). The shorter one focuses on the coating of specific areas of negative charges on the protein and the latter one exceeds the protein size by more than 20 times and would thus act as a crosslinker. In the second set, the protein was coated with negatively charged tailor-made polymers. Dextrans of different molecular weight were modified with a high density of aspartic acid groups (Dext6kDa and Dext2000kDa), the former with a suitable size especially for the coating of particular areas with positively charged residues in the protein (Fig. S3†) and the latter once again much larger than the protein.

CALB modified with PEI polymers were used for Ag nanobiohybrid synthesis using the same protocol, as previously described. Surprisingly, the synthesis using CALB–PEI0.8kDa conjugate showed a pH >10, and XRD confirmed the formation of Ag(0) species. Using the CALB–PEI750kDa conjugate, the main silver species was Ag<sub>2</sub>O as being observed using the non-modified enzyme (Fig. S4†).

In the second approach, tailor-made dextran polymers were prepared as previously reported.<sup>35</sup> These polymers have been recently used for stabilization of multimeric enzymes,<sup>19</sup> and also, we observed important influences on the selectivity and specificity of enzymes after their modification.<sup>18,36,37</sup> Dextrans

with molecular weights of 6 kDa and 2000 kDa, respectively, were modified firstly using sodium periodate to create dextran-aldehyde (Dext-Asp). The chemical incorporation of aspartic acid molecules into dextran-aldehyde polymer resulted in the final dextran-aspartic acid polymers called Dext6kDa and Dext2000kDa. Then, these polymers were used for the coating of CALB by the ionic exchange between carboxylic groups of the polymer and amino groups of the protein to obtain CALB–Dext6kDa and CALB–Dext2000kDa conjugates. The modification was performed at neutral pH, conditions, where the N-terminal group and other residues such as Arg and Lys were positively charged. Indeed, analyzing the structure of the protein, the main area with positive charges around the N-terminus, which is located opposite to the active site of the enzyme, was observed. This represents a preferred area of formation of salt bridges with the negatively charged polymers (Fig. S3†).

These bioconjugates were used for the preparation Ag-nanobiohybrids (Fig. 4, 5 and Fig. S5, 6†). The pH was adjusted and it was conserved around 5. During the incubation, a heterogeneous material was formed in high amounts (>100 mg) in both cases.

In the nanobiohybrid synthesized using CALB–Dext6kDa, the XRD analysis revealed the prevalent formation of Ag(0) species, based on the face-centered cubic structure (JCPDS, File No. 04-0783),<sup>38</sup> with Ag<sub>2</sub>O as a minor component (Fig. 4a).

The formation of crystalline spherical nanoparticles was confirmed by transmission electron microscopy (TEM) analysis (Fig. 4c). Silver nanoparticles with a diameter average size of around 8 nm were obtained (Fig. 4c and d). This result showed the formation of slightly smaller silver nanoparticles than using the unmodified enzyme. In this case, also the bioconjugate enzyme acted as an *in situ* reducing agent.

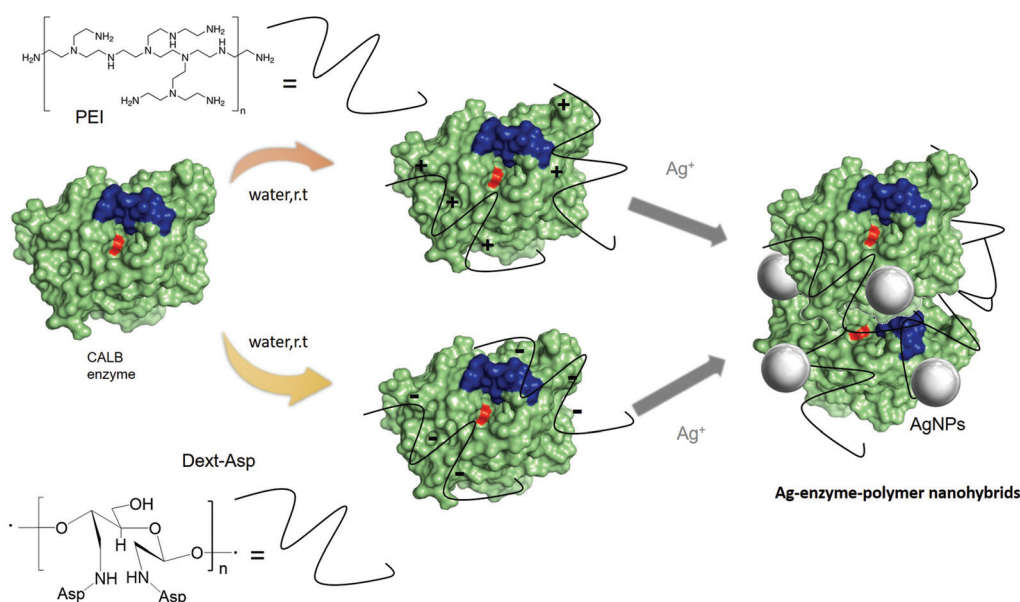


Fig. 3 Preparation of Ag-nanobiohybrids using enzyme–polymer conjugates.





Fig. 4 Synthesis of AgNPs-CALB-6kDa. (a) XRD pattern. (b) SEM image. (c) TEM (inset HRTEM) and IFFT images. (d) Particle size distribution.

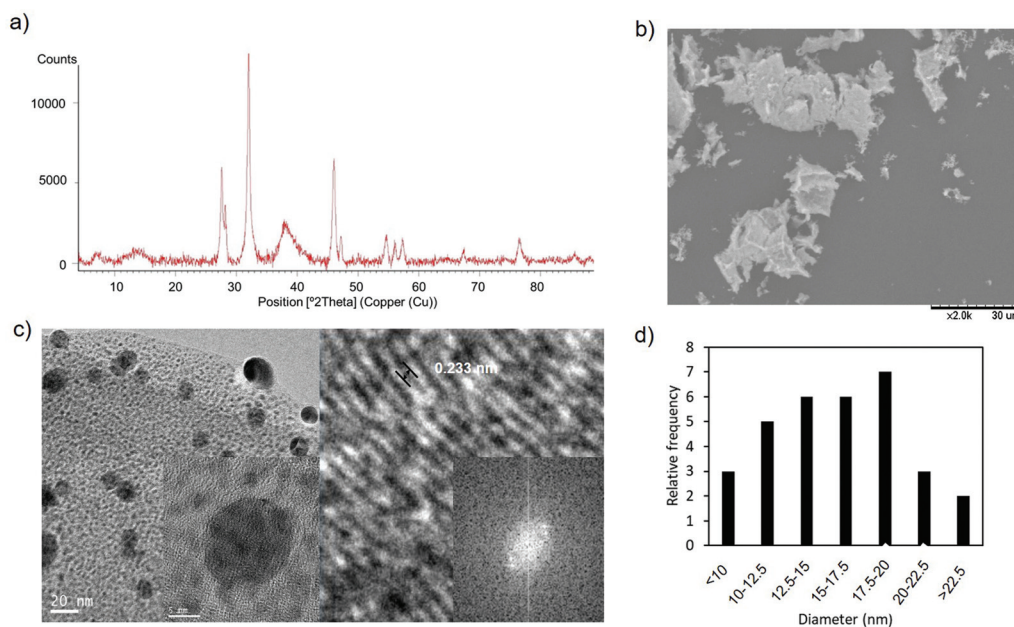


Fig. 5 Synthesis of AgNPs-CALB-Dext2000kDa. (a) XRD pattern. (b) SEM image. (c) TEM (inset HRTEM) and IFFT images. (d) Nanoparticle size distribution.

Using the bioconjugate CALB-Dext2000kDa as the basis for the nanohybrids, the XRD analysis indicated the presence of Ag<sub>2</sub>O and Ag(0) and also AgO species (peaks at 27° and 48°, respectively) in this nanobiohybrid, implying that oxidation of silver(I) oxide to silver(II) oxide is taking place in the presence of the huge-size polymer (Fig. 5a).

The analysis through TEM microscopy revealed the formation of well-monodispersed spherical nanoparticles (Fig. 5c and Fig. S6†) with an average diameter size of 14 nm (Fig. 5d). The presence of polymer in the conjugate generated a larger protein, allowing the growth of silver nanoparticles, compared to those prepared by using simply CALB (Fig. 2). XPS analysis



was performed in order to confirm the presence of the different silver species (Fig. S7†).

This initial systematic comparison of coating additives clearly illustrates how the nature of the polymer–protein conjugate affects the silver species in terms of the oxidation state, size and distribution. The overall silver content in nanobiohybrids, on the other hand, seemed to be widely independent of the potential additives (as determined by ICP-OES) relative to the unmodified CALB.

Next, the role of the protein structure in the formation of silver nanoparticle hybrids was studied. At this point, the lipase of *Thermomyces lanuginosus* (TLL) was used as an alternative protein matrix. This enzyme shows a similar size to CALB in its monomeric form, however, it has a greater tendency to aggregate and to generate multimeric systems.<sup>39</sup> Indeed, recently, we have demonstrated how this enzyme showed an impressive effect on the synthesis of iron nanobiohybrids, where completely different iron species and nanostructure morphologies were observed using TLL as a template when compared to CALB.<sup>17</sup>

In the case of TLL, the silver nanobiohybrids were synthesized in the absence and in the presence of cetyltrimethylammonium bromide (CTAB). This cationic detergent allowed control of the size of the protein as it assists in retaining the monomeric form, and generating a dramatic increase in the lipase activity.<sup>40</sup>

However, the silver nanobiohybrids were obtained in both cases in a very similar way (Fig. 6 and Fig. S8, 9†). Ag<sub>2</sub>O nanoparticles were produced as confirmed by XRD. A small difference was observed in the TEM analysis of the size of the nanoparticles, with a 16 nm average diameter size in the presence of CTAB, because of the coordination effect of the detergent onto the protein surface. In both cases, the content of silver calculated by ICP-OES analysis was 33%.

Overall, comparing the outcome in the nanobiohybrid synthesis using CALB and TLL, respectively, no significant differences in the nature of the silver species or the nanoparticle size were observed, and only in the presence of CTAB larger nanoparticles were formed in TLL. However, the content of silver in the TLL hybrids was higher than that with CALB.

This phenomenon could be explained by considering the structure of both proteins, especially the groups that silver ions can coordinate (Fig. 7). The nanoparticle formation mechanism involves initial coordination between amino acids of the protein and the metal ions. In this way, it has been described that they coordinate with carboxyl groups in different ways (Fig. 7c).<sup>41</sup>

Comparing the extent of accessible Asp and Glu residues of both proteins, we can see how the TLL effectively presents a greater number of these anionic residues (up to 31 carboxylate groups) (Fig. 7b). Alongside the carboxylates, another functional group with high coordination capacity for silver ions is



Fig. 6 Characterization of synthesized TLL–Ag nanobiohybrids. (a) TEM image of TLL–Ag. (b) Nanoparticle size distribution of TLL–Ag (a small fraction). (c) TEM image of TLL–AgCTAB. (d) Nanoparticle size distribution of TLL–AgCTAB.







**Fig. 7** (a) 3D surface of CALB with its critical amino acid residues marked. Asp and Glu residues (yellow), His (cyan). (b) 3D surface of TLL with its critical amino acid residues marked. Asp and Glu residues (yellow), His (cyan). (c) Proposed silver coordination species induced by the protein. Pymol program using PDB file TCA and 1DTE were used to prepare the figure.

the cysteine thiol. CALB does not feature any Cys in its peptide sequence, whereas, in TLL, cysteines are present, giving additional anchor points.

An advantage of silver coordination over other metals is the possible coordination modes with carboxylate groups, where both a single atom or two atoms per functional group can be coordinated (Fig. 7c).

Regarding the size of the nanoparticles, the results have shown that mainly the modification of this parameter can be controlled by means of the previous modification of the protein with polymers or the presence of detergents.

### Synthesis and characterization of Au nanoparticles–enzyme hybrid

Following the results obtained with silver, novel Au nanobiohybrids were synthesized using unmodified enzyme or CALB conjugated with Dext6kDa as a protein matrix (Fig. 8). In this case, the redox potential of Au allowed in all cases the formation of exclusively metallic Au species in the different Au nanobiohybrids, as confirmed by XRD analysis (Fig. 8b).

In the preparation of the Au nanohybrids, an important parameter was the pH of the gold solution. Tetrachloroaurate (III) ( $\text{HAuCl}_4$ ) was used as a gold source that was dissolved in water and then pH adjusted to 6 or 4.5, respectively. Subsequently, an aqueous enzyme solution was added and after incubation, the hybrid was obtained. During the course of the reactions, the pH of the solution decreased to a final pH of 4.4 in the first case, while in the latter, the pH dropped down to very acidic conditions (pH 1.9). This obviously had

consequences on the final formation of the nanobiohybrid. ICP-OES analysis of the two individual nanobiohybrids showed that the content of Au in each case was very different. While in the first case it barely exceeded 1%, in the second case, an Au content of 16% was reached.

These results could indicate that the gold coordination with the protein proceeds in a different way than silver. It has been reported that gold has a high affinity of coordination with protonated Asp-(H<sup>+</sup>) or Glu-(H<sup>+</sup>) via the nitrogen of the amino group, where the metal ions with high Lewis acidity cause deprotonation and consequently a lower pH in the final solution.<sup>42</sup> Also, high affinity is found with Tyr, which is a residue present in the CALB structure (Fig. S10†).

Furthermore, the nature of the nanoparticles in **AuNPs–CALB–pH4.5** was evaluated (Fig. 9). TEM analysis revealed the formation of nanoparticles with different forms, mainly spherical (Fig. 9), and with two different ranges of size, with an average of 18 nm (the smallest ones) and another one with more than 100 nm diameter size nanoparticles (Fig. 9).

Next, the preparation of Au nanobiohybrid was performed using CALB–Dext6kDa conjugate with gold solution adjusted at acidic pH (Fig. 10 and Fig. S11†). As previously described with silver, a good amount of solid was obtained; in this case, the final pH on the solution was more acidic (pH 3). However, in comparison with the former Au hybrid, the metal content determined by ICP-OES accounted for 4%. Evaluating the protein structure (Fig. S12†), we can observe that the positively charged residues at these conditions (Arg, Lys), which are involved in the coordination with the polymer in the conju-





Fig. 8 Preparation of Au-nanobiohybrids. (a) Synthetic scheme. (b) XDR pattern of nanohybrids.



Fig. 9 Characterization of the synthesized AuNPs-CALB-pH4.5 hybrid. (a) TEM images. (b) Nanoparticles size distribution.

gation formation, also could form salt bridges with carboxylate residues on the protein. As a potential result, this modified enzyme may exhibit a lower ability for coordination with Au, which would translate to a lower final relative content of the metal.

TEM analysis of the AuNPs-CALB-Dext6kDa hybrid showed the formation of mainly three different nanoparticle structures, spherical nanoparticles with two kinds of sizes, one

smaller with an average diameter size of 9.7 nm and other larger with an average of 22 nm, and also nanorods with 20–30 nm and 45–50 nm length (Fig. 10).

Also, this result clearly underlines the possible effects of the coating on the enzyme for the final metallic nanostructure distribution, which in general are much smaller than the nanobiohybrids synthesized with the unmodified enzyme.







Fig. 10 Characterization of synthesized AuNPs-CALB-Dext6kDa hybrid. (a) TEM images. (b) Nanoparticles size distribution.

As in the Ag nanobiohybrid, the effect of using another enzyme was tested. In this case, when TLL was used, certain differences were observed. The content of Au of 19% (by ICP) was slightly higher than that using CALB. The pH of the solution after 24 h incubation was also somewhat less acidic than that using CALB (3.6). These results can be explained considering the isoelectric point of TLL (pI 4.4) compared to that of CALB (pI 6), which means that although the former contains more Asp/Glu residues in the structure, not all of them are in deprotonated form for coordination with Au.

The mechanism of coordination of Au is different from that of Ag, and in general, neutral Asp and Glu bind  $\text{Au}^+$  solely through the nitrogen of the amino group, while the deprotonated anionic variants of these amino acids bind  $\text{Au}^+$  through both the nitrogen and one of the oxygens of the carboxylate group. Also, a monodentate complex with  $\text{Au}^+$  is formed in the case of aliphatic amino acids (except Met), Asp, Glu, Pro, Ser, and Thr.<sup>42</sup> However, even though the amount of gold was similar, clear differences were observed in terms of nanoparticle formation. TEM analysis revealed two different structures, spherical nanoparticles with an average diameter size of 5.9 nm, the smallest observed for gold in these nanobiohybrids, but also nanoflowers with around 100–200 nm diameter (Fig. 11 and Fig. S13†).

#### Determination of enzyme and metallic activity of nanobiohybrids

**Metallic activity of nanobiohybrids.** The catalytic efficiency of different Ag and Au nanoparticle-enzyme hybrids was tested in the chemoselective hydrogenation of *p*-nitrophenol (*p*NP) to *p*-aminophenol (*p*AP) (Table 1). The reaction was carried out in aqueous media and at room temperature. Free CALB and TLL solutions were tested as controls, and no activity was found in any case (data not shown).

For Ag nanobiohybrids, the highest efficiency was found with the AgNPs-CALB hybrid, with a TOF value of  $22 \text{ h}^{-1}$ . However, from all the hybrids with bioconjugated proteins, AgNPs-CALB-Dext6kDa showed the best results, with 93% conversion in 5 min ( $7.6 \text{ h}^{-1}$  TOF value) (Table 1, entry 4). The lowest results were found with AgNPs-CALB-PEI750kDa, whereas, after changing the enzyme, the hybrid AgNPs-TLL showed 10 times lower catalytic efficiency. This could be explained considering the higher size of  $\text{Ag}_2\text{O}$  nanoparticles and maybe the dispersion in the protein matrix, with a better, more even distribution in the CALB matrix.

For the CALB hybrids, it seems that the  $\text{Ag}_2\text{O}$  species showed higher catalytic efficiency in this reaction than Ag.<sup>43</sup> This could explain why the AgNPs-CALB-Dext6kDa with smaller mixed nanoparticles of Ag/ $\text{Ag}_2\text{O}$  was a less active catalyst than the AgNPs-CALB hybrid. The valence of Ag atoms also synergistically affects the rate of reduction, because of the positive charge of  $\text{Ag}^+$  benefiting the adsorption of both negatively-charged reactants of 4-nitrophenolate and  $\text{BH}_4^-$  anions.<sup>43</sup>

In the case of Au nanobiohybrids, the one prepared using the bioconjugate CALB-Dext6kDa showed more than 10 times higher activity than its counterpart derived from unmodified CALB (Table 1), with a TOF value of  $300 \text{ h}^{-1}$ . In this case, the AuNPs-TLL hybrid showed a similar efficiency as AuNPs-CALB (Table 1 entries 8 and 10). This result could be explained considering the smallest Au(0) nanostructures (particles and rods) in the AuNPs-CALB-Dext6kDa. The hybrid showed excellent stability at room temperature for months, without the loss of activity or selectivity.

**Enzymatic activity of nanobiohybrids.** The second important parameter for developing cascade reactions with these nanohybrids is to make sure that the activity by the enzyme biocatalyst is retained during the hybrid formation. In order to assess the residual lipase activity of the protein matrices, the enzy-



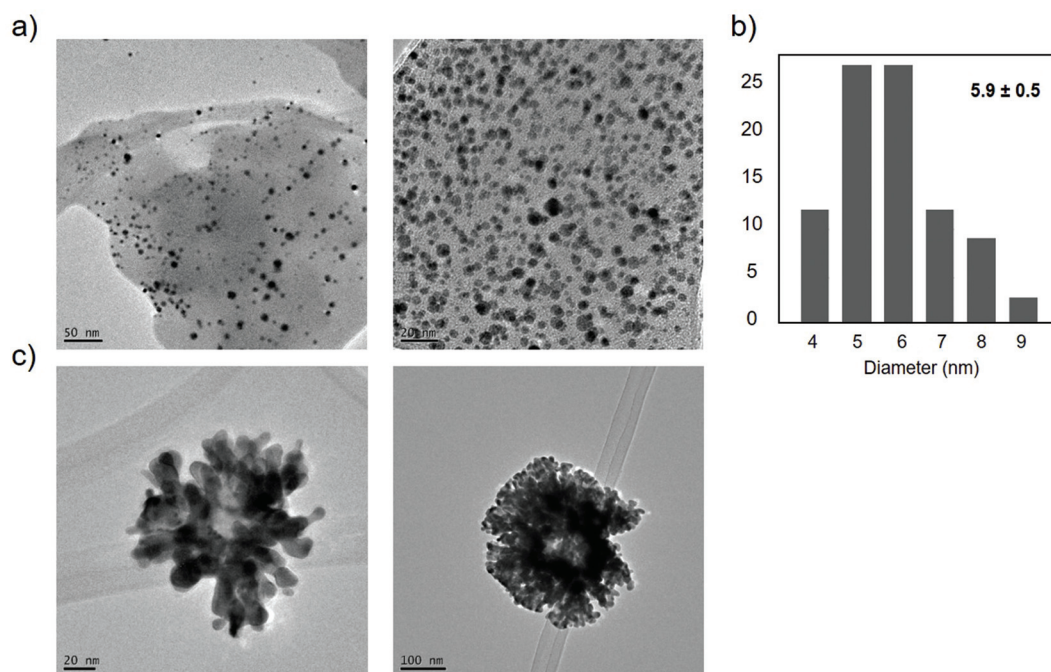


**Fig. 11** Characterization of synthesized AuNPs-TLL hybrid. (a) TEM images of nanoparticles. (b) Nanoparticles size distribution. (c) TEM images of nanoflowers.

**Table 1** Hydrogenation of *p*-nitrophenol catalysed by Ag and AuNPs-enzyme hybrids<sup>a</sup>

| Entry | Catalyst               | Time (min) | Cat Amount (mg) | Metal amount <sup>b</sup> (%) per mg | Yield of <i>p</i> AP (%) | TOF value <sup>c</sup> (h <sup>-1</sup> ) |
|-------|------------------------|------------|-----------------|--------------------------------------|--------------------------|---|
| 1     | AgNPs-CALB             | 1          | 2               | 26                                   | >99                      | 23.0                                      |
| 2     | AgNPs-CALB-PEI0.8kDa   | 5          | 1.5             | 24                                   | 62                       | 4.4                                       |
| 3     | AgNPs-CALB-PEI750kDa   | 15         | 2               | 26                                   | 13                       | 0.2                                       |
| 4     | AgNPs-CALB-Dext6kDa    | 5          | 1.5             | 21                                   | 93                       | 7.6                                       |
| 5     | AgNPs-CALB-Dext2000kDa | 5          | 2               | 26                                   | 85                       | 4.2                                       |
| 6     | AgNPs-TLL              | 5          | 1               | 33                                   | 37                       | 2.9                                       |
| 7     | AgNPs-TLL-CTAB         | 5          | 2               | 33                                   | 49                       | 1.9                                       |
| 8     | AuNPs-CALB-pH4.5       | 2.5        | 2               | 15.8                                 | 94                       | 28  |
| 9     | AuNPs-CALB-Dext6kDa    | 1          | 2               | 4.1                                  | 100                      | 300                                       |
| 10    | AuNPs-TLL-pH 4.5       | 2          | 2               | 19.2                                 | 85                       | 29  |

<sup>a</sup> Conditions: 1.0 mM (3 mg) **1**, 40 mM (3 mg) NaBH<sub>4</sub>, 2 mL of distilled water, air and room temperature. <sup>b</sup> Determined by ICP-OES. <sup>c</sup> TOF value was defined as the moles of **2** per mole of noble metal atoms in the nanocatalyst per hour.

matic activity of each hybrid was evaluated based on the performance in the hydrolysis assay using *p*-nitrophenyl propionate (**3**) (Table 2).

In most of the cases, the activity of the enzyme in the hybrid for this assay was reduced compared to that of the free enzyme. However, in almost all cases (except for AgNPs-CALB-Dext2000kDa) enzymatic activity was observed in the hybrid catalysts (Table 2).

The AgNPs-CALB hybrid conserved the highest enzymatic activity (Table 2, entry 1) among all hybrids (also showing the highest metallic activity (Table 1). In this case, the bioconjugation affected the reduction of the final value of the enzymatic activity. Also, a hybrid synthesized with TLL showed activity, which is quite interesting because this enzyme presents a very low activity towards this substrate.<sup>40</sup> The nanobiohybrid synthesized using CTAB, a strategy used for conserving more



**Table 2** Hydrolysis of **3** catalyzed by Ag or AuNPs–enzyme hybrids<sup>a</sup>


| Entry | Catalyst               | Catalyst concentration (mg ml <sup>-1</sup> ) | Catalyst amount (μg) | Enzymatic specific activity <sup>b</sup> |
|-------|------------------------|---|----------------------|--|
| 1     | AgNPs–CALB             | 0.4   | 8                    | 0.3                                      |
| 2     | AgNPs–CALB–PEI0.8kDa   | 1.1   | 22                   | 0.09                                     |
| 3     | AgNPs–CALB–PEI750kDa   | 4.1   | 82                   | 0.035                                    |
| 4     | AgNPs–CALB–Dext6kDa    | 2.2   | 44                   | 0.011                                    |
| 5     | AgNPs–CALB–Dext2000kDa | 2.3   | 46                   | 0  |
| 6     | AgNPs–TLL              | 1.7   | 170                  | 0.023                                    |
| 7     | AgNPs–TLL–CTAB         | 1.6   | 160                  | 0.021                                    |
| 8     | AuNPs–CALB–pH4.5       | 3.2   | 64                   | 0.105                                    |
| 9     | AuNPs–CALB–Dext6kDa    | 5.5   | 110                  | 0.035                                    |
| 10    | AuNPs–TLL–pH 4.5       | 1.7   | 170                  | 0.031                                    |

<sup>a</sup> Conditions: 0.4 mM **3**, 20 μl (CALB hybrids) or 100 μl (TLL hybrids) suspension, 2.5 mL of 25 mM sodium phosphate buffer pH 7 or distilled water, air and room temperature. <sup>b</sup> The enzymatic specific activity (nmol of hydrolyzed **3** per minute per mg of hybrid) of the nanobiohybrids were calculated as described in the experimental section.

activity in the enzyme,<sup>40</sup> did not differ much in its final activity value (Table 2, entry 7).

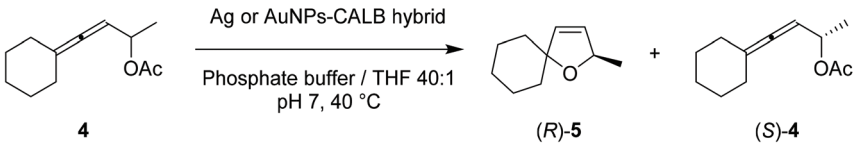
### Cascade reaction catalyzed by dual-active Ag and Au nanobiohybrids

After observing the preservation of both the enzyme and metallic activity in the generated Ag and Au nanohybrids, we evaluated them as dual-activity heterogeneous catalysts in a cascade reaction to produce enantioenriched dihydrofurans from allenic acetates. Here, the process begins with kinetic resolution hydrolysis of racemic allenic acetate **4** induced by the lipase activity of the nanobiohybrid. The thus-obtained enantiopure allenic alcohol intermediate is subsequently cycloisomerized *via* the Ag or Au activity of the nanohybrid to form 2,5-dihydrofuran (*R*)-**5** as an optically pure enantiomer.

Firstly, the lipase–AgNPs hybrids were evaluated in the hydrolytic cyclization of allenic acetate **4** into dihydrofuran (*R*)-**5** (Table 3). The AgNPs–CALB hybrid gave an encouraging conversion of 26% and good enantioselectivity (88% ee) of the desired furan cascade product (*R*)-**5** (Table 3, entry 1). Silver nanohybrids synthesized using polyethyleneimine bioconjugates failed to produce effective catalysts for this transformation, catalysing only minor conversions into (*R*)-**5** (data not shown).

AgNPs–CALB–Dext6kDa and AgNPs–CALB–Dext2000kDa hybrids showed excellent catalytic performance, with almost 50% conversion and excellent enantioselectivity (94–95% ee) of (*R*)-**5**.

Next, the gold nanoparticle biohybrids were also examined as mediators for the cascade reaction. The AuNPs–CALB–pH4.5 hybrid (Table 3, entry 4) performed faster than the ana-

**Table 3** Evaluation of lipase–silver and gold nanoparticle hybrids in hydrolysis/cyclization of allenic acetate **4**<sup>a</sup>


| Entry | Catalyst               | Time (d) | Conversion <sup>b</sup> (%) | ( <i>R</i> )- <b>5</b> , ee <sup>b</sup> (%) | ( <i>S</i> )- <b>4</b> , ee <sup>b</sup> (%) |
|-------|------------------------|----------|-----------------------------|--|--|
| 1     | AgNPs–CALB             | 4        | 26                          | 88   | 88   |
| 2     | AgNPs–CALB–Dext6kDa    | 3        | 43                          | 94   | 94   |
| 3     | AgNPs–CALB–Dext2000kDa | 3        | 42                          | 95   | 84   |
| 4     | AuNPs–CALB–pH4.5       | 2        | 21                          | 93   | 64   |
| 5     | AuNPs–CALB–Dext6kDa    | 3        | 2                           | 93   | 99   |

<sup>a</sup> Conditions: 40 μmol (7.8 mg) **4**, 1.5 mg CALB hybrid, 20 μl THF, 0.8 mL phosphate buffer (0.1 M, pH 7), 40 °C. <sup>b</sup> Conversion and % ee were determined using chiral GC.





logous Ag hybrid, reaching a similar conversion of 21% and a great optical purity of 93% in half the reaction time compared to **AgNPs-CALB**. However, longer reaction times using the Au biohybrid resulted in lower recovery of the desired (*R*)-5, indicating consumption of the product through unidentified side-reactions in the Au-catalyzed process. Similar behavior was observed using **AuNPs-CALB-Dext6kDa**, which very efficiently catalyzes the purification of the unreacted allenic acetate enantiomer (*S*)-4 to 99% ee, but no significant amounts of 2,5-dihydrofuran (*R*)-5 or the intermediate allenic alcohol were obtained after the reaction (Table 3, entry 5).

The Ag and Au nanobiohybrids constructed using TLL instead of CALB also showed some activity towards the cascade process, however, in rates not sufficient for significant conversion in reasonable incubation times.

## Conclusions

A novel strategy has been developed to synthesize silver and gold nanoparticles–enzyme hybrids with good control of metal species, nanoparticles size and morphology. It was demonstrated that silver or gold nanohybrids were produced in a different way in terms of protein coordination, affecting, especially, the final metal species. In all the cases, the nanoparticle formation in the protein matrix was induced *in situ* by the enzyme, without the necessity to use an external reducing agent. Enzyme–polymer conjugates directly induced the formation of smaller nanoparticles in both metal systems, and in the gold hybrid, the formation of nanoparticles and nanorods was found. Most of the synthesized hybrids maintained (dual) enzymatic and metallic activities. Finally, these dual activity catalysts were successfully used in the stereoselective hydrolysis/cyclization cascade reaction to produce a 2,5-dihydrofuran in excellent conversion and enantiopurity from an allenic acetate. These results demonstrate the high applicability of these novel hybrids in cascade reactions by exploiting the multiple activities retained in the designer catalysts. Future research will aim at expanding both the reaction scope and the number of catalytic activities within the nanobiohybrids in order to enable more efficient and sustainable processes to complex synthetic target structures for pharmaceuticals and fine chemicals.

## Experimental

### General

*Candida antarctica* B lipase (Lipozyme® CALB) (CALB), *Thermomyces lanuginosus* lipase (TLL) solution (Lipozyme® TL 100L) was from Novozymes (Denmark). Silver nitrate, gold(III) chloride trihydrate ( $\text{HAuCl}_4 \cdot 3\text{H}_2\text{O}$ ), branched polyethyleneimines (PEI) ( $M_w = 800$  Da or  $M_w = 2000$  kDa) (approx. the molar ratio of primary/secondary/tertiary amine = approx. 1/1.2/0.76), dextrans ( $M_w$ : 6 kDa or 2000 kDa), aspartic acid, sodium periodate, *p*-nitrophenol and *p*-aminophenol were pro-

vided by Sigma-Aldrich. Acetonitrile HPLC grade was provided by Scharlab. Dextran-aspartic acid polymers (Dext 6kDa and Dext 2000kDa) were synthesized as previously reported.<sup>35</sup>

Inductively coupled plasma atomic emission spectrometry (ICP-OES) was performed using a PerkinElmer OPTIMA 2100 DV equipment. X-ray photoelectron analysis (XPS) was carried out on a SPECS GmbH spectrometer equipped with a Phoibos 150 9MCD energy analyzer. A nonmonochromatic magnesium X-ray source with a power of 200 W and voltage of 12 kV was used. The X-Ray diffraction (XRD) pattern was obtained using a Texture Analysis Diffractometer D8 Advance (Bruker) with Cu  $K\alpha$  radiation. Transmission electron microscopy (TEM) and high-resolution TEM microscopy (HRTEM) analysis were performed on a JEOL 2100F microscope equipped with an EDX detector INCA x-sight (Oxford Instruments). To recover the nanobiohybrids, a Biocen 22 R (Orto-Alresa, Spain) refrigerated centrifuge was used. The spectrophotometric analyses were run on a V-730 spectrophotometer (JASCO, Japan). An HPLC spectrum P100 (Thermo Separation products) was used. Analyses were run at 25 °C using an L-7300 column oven and a UV6000LP detector. Lyophilization of the hybrids was performed using a Telstar LyoQuest laboratory freeze-dryer. NMR, GC and optical rotation were recorded at the School of Chemical Engineering of Aalto University.  $^1\text{H}$  and  $^{13}\text{C}$  NMR spectra were recorded with a Bruker Avance NEO 400 ( $^1\text{H}$  400.13 MHz,  $^{13}\text{C}$  100.62 MHz). The chemical shifts are reported in parts per million (ppm) in relation to non-deuterated chloroform signal ( $^1\text{H}$  NMR:  $\delta = 7.26$ ;  $^{13}\text{C}$  NMR:  $\delta = 77.16$ ). Gas chromatography was performed on a Shimadzu GC-2010 Plus gas chromatograph with a Supelco Analytical Beta DEX 120 column (30 m  $\times$  0.25 mm), using 2.55 mL min<sup>-1</sup> column flow and temperature program: 50 °C (2 min)/20 °C min<sup>-1</sup>/115 °C (35 min). Optical rotations were measured using an Autopol VI Automatic Polarimeter from Rudolph Research Analytical.

### Preparation of polymer–lipase conjugates

0.8 mL commercial CALB solution (9.57 mg mL<sup>-1</sup> protein concentration determined by Bradford assay) was dissolved in 15 mL distilled H<sub>2</sub>O. Then, solid 79 mg polymer (PEI (800 Da), Dext6kDa or Dext200kDa) or 152 mg of PEI2000kDa (50 wt% in H<sub>2</sub>O) was added to the protein solution and the mixture was maintained by roller stirring for 20 min at room temperature.

### General synthesis of Ag nanoparticles–enzyme hybrids

0.8 mL commercial CALB solution (9.57 mg mL<sup>-1</sup> protein) was added to 15 mL distilled H<sub>2</sub>O. Then, 10 mL of silver nitrate solution (water) (50 mg mL<sup>-1</sup>) was added to the 15 mL of CALB solution (described above) or CALB-polymer conjugates solution. The mixture was stirred at room temperature for 24 or 43 hours. The formed solid material was collected from the resulting suspension by centrifugation and it was washed twice with 10 mL distilled H<sub>2</sub>O. Finally, the pellet was re-suspended in 2 mL of water, collected in a cryotube, frozen with liquid nitrogen and lyophilized for 16 hours, obtaining the following solid Ag nanobiohybrids: **AgNPs-CALB** (9.8 mg of dark



brown), **AgNPs-CALB-PEI-0.8kDa** (26 mg dark brown), **AgNPs-CALB-PEI-750kDa** (102 mg reddish brown), **AgNPs-CALB-Dext-6kDa** (54.3 mg reddish brown), **AgNPs-CALB-Dext-2000kDa** (58.0 mg reddish brown).

In the case of TLL, 1.0 mL commercial TLL solution (29.8 mg mL<sup>-1</sup> protein) was added to 20 mL distilled H<sub>2</sub>O, with or without the presence of 1.0 mg cetyltrimethylammonium bromide (CTAB) (0.005 wt%), followed by the addition of 0.40 g AgNO<sub>3</sub>. The procedure was the same as previously described by CALB hybrids. The nanohybrids synthesized were: **AgNPs-TLL** (33 mg reddish brown), **AgNPs-TLL-CTAB** (31 mg reddish-brown).

Characterization of different nanobiohybrids was performed using XRD, ICP-OES, SEM and TEM analysis.

Table S1† summarizes all the different Ag hybrids synthesized.

### General synthesis of Au nanoparticles–enzyme hybrids

Gold(III) chloride trihydrate (205 mg) was dissolved in distilled water (10 mL) and then the solution was adjusted at pH 6, pH 4.5, or pH 5 using 1 M NaOH. 3 mL commercial CALB solution (9.57 mg mL<sup>-1</sup> protein) or 1 mL commercial TLL solution was added to 10 mL distilled H<sub>2</sub>O. Then, 10 mL of enzyme solution was added to 10 mL of gold solution (20 mg mL<sup>-1</sup>) at different adjusted pHs, CALB (solution at pH 6, pH 4.5), TLL (solution at pH 4.5), CALB-Dext6kDa (solution at pH 5). The mixture was stirred at room temperature for 24 hours. The formed solid material was collected from the resulting suspension by centrifuge and it was washed twice with 10 mL distilled H<sub>2</sub>O. Finally, the pellet was re-suspended in 2 mL of water, collected in a cryotube, frozen with liquid nitrogen and lyophilized for 16 hours, obtaining the following solid Au nanobiohybrids: **AuNPs-CALBpH6** (30.6 mg dark brown), **AuNPs-CALB-pH4.5** (63.9 mg brown), **AuNPs-CALB-Dext-6kDa** (109.9 mg black solid), **AuNPs-TLL-pH4.5** (34.8 mg light brown color).

Table S1† summarizes all the different Au hybrids synthesized.

### Metallic activity assay: reduction of 4-nitrophenol (1) to 4-aminophenol (2)

*p*-Nitrophenol (1) was dissolved in 2 mL of distilled water at 1 mM concentration. Then, solid NaBH<sub>4</sub> (3.2 mg) was added to the solution. After this addition, the light-yellow solution changes to a strong yellow colour, generating the formation of 4-nitrophenolate ions (substrate UV-peak undergoes an immediate shift from 317 to 400 nm). After 30 seconds, 3 mg of the different Au and Ag nanobiohybrids were added under gentle stirring at room temperature in an orbital shaker. The reaction progress was monitored by taking out an aliquot of the solution (0.1 mL) at different times, diluting it with distilled water (2 mL) and measuring the absorption spectrum between 500 and 300 nm in a quartz cuvette.

### Lipase activity assay: hydrolysis of *p*-nitrophenyl propionate (3) to *p*-nitrophenol (1)

The enzymatic activity of the Ag and Au nanobiohybrids was analyzed spectrophotometrically measuring the increment in

absorbance at 348 nm produced by the release of *p*-nitrophenol (1) ( $\epsilon = 5.150 \text{ M}^{-1} \text{ cm}^{-1}$ ) in the hydrolysis of 0.4 mM 3 in 25 mM sodium phosphate at pH 7 and 25 °C. To initialize the reaction, 0.02 or 0.1 mL of lipase hybrid suspension was added to 2.5 mL of substrate solution under magnetic stirring. Enzymatic activity is given as nmol of hydrolyzed 3 per minute per mg of hybrid (IU) under the conditions described above. In the reactions involving Ag-salts, distilled water was used instead of the sodium phosphate buffer solution.

### General lipase-hybrid catalyzed kinetic resolution hydrolysis/cyclization

Racemic allenic acetate 4-cyclohexylidenebut-3-en-2-yl acetate 4 was prepared as reported previously.<sup>33</sup>

The allenic acetate 4 (7.8 mg, 40  $\mu\text{mol}$ ) in 20  $\mu\text{L}$  tetrahydrofuran was added into a 0.8 mL phosphate buffer solution (0.1 M, pH 7.0). Solid lipase-metal nanobiohybrid (1.5 mg) was added to the solution. The resulting suspension was shaken at 800 rpm at 40 °C for 2–4 days. Then, the mixture was extracted with ethyl acetate (4  $\times$  1 mL). The remaining solid materials were removed from the combined organic layers by filtration. The filtrate was analyzed by gas chromatography to determine the conversion and purity of the products. The retention times of the compounds were compared to those of synthesized racemic mixtures of the compounds (Fig. S14†).

**4-Cyclohexylidenebut-3-en-2-yl acetate (4).** <sup>1</sup>H NMR (400 MHz, CDCl<sub>3</sub>):  $\delta$  [ppm] = 5.32 (dq,  $J = 6.4, 5.5$  Hz, 1H), 5.10 (dq,  $J = 5.5, 2.1$  Hz, 1H), 2.18–2.05 (m, 4H), 2.04 (s, 3H), 1.67–1.49 (m, 6H), 1.30 (d,  $J = 6.4$  Hz, 3H). <sup>13</sup>C NMR (100 MHz, CDCl<sub>3</sub>):  $\delta$  [ppm] = 198.4, 170.6, 105.7, 90.6, 69.4, 31.4, 31.4, 27.5, 27.5, 26.2, 21.6, 19.9. (*S*)-4 (94% ee);  $[\alpha]_D^{25}$ : –54.8 ( $c$  1.10, CH<sub>2</sub>Cl<sub>2</sub>) (Fig. S15†).

**2-Methyl-1-oxaspiro[4.5]dec-3-ene (5).** <sup>1</sup>H NMR (400 MHz, CDCl<sub>3</sub>):  $\delta$  [ppm] = 5.87 (dd,  $J = 6.1, 2.1$  Hz, 1H), 5.70 (dd,  $J = 6.1, 1.4$  Hz, 1H), 4.90 (qdd,  $J = 6.4, 2.1, 1.4$  Hz, 1H), 1.75–1.63 (m, 2H), 1.61–1.53 (m, 4H), 1.50–1.38 (m, 4H), 1.25 (d,  $J = 6.4$  Hz, 3H). <sup>13</sup>C NMR (100 MHz, CDCl<sub>3</sub>):  $\delta$  [ppm] = 133.4, 130.4, 89.6, 80.5, 39.6, 37.6, 25.6, 23.7, 23.6, 23.4. (*R*)-5 (94% ee);  $[\alpha]_D^{25}$ : –53.1 ( $c$  0.48, CH<sub>2</sub>Cl<sub>2</sub>). (Fig. S16†).

## Conflicts of interest

There are no conflicts to declare.

## Acknowledgements

The authors thank the support of the Spanish National Research Council (CSIC). We gratefully acknowledge financial support by the Suomen Akatemia (grant numbers 298250 & 324976, J. D.), the COST action CA15106 (CHAOS) and Finnish Foundation for Technology Promotion. We also thank Ramiro Martínez from Novozymes.



## References

- 1 H. Pellissier, Enantioselective Silver-Catalyzed Transformations, *Chem. Rev.*, 2016, **116**, 14868–14917.
- 2 D. Pflästerera and A. S. K. Hashmi, Gold catalysis in total synthesis – recent achievements, *Chem. Soc. Rev.*, 2016, **45**, 1331–1367.
- 3 A. G. Tathe, Urvashi, A. K. Yadav, C. C. Chintawar and N. T. Patil, Gold-Catalyzed 1,2-Aminoarylation of Alkenes with External Amines, *ACS Catal.*, 2021, **11**, 4576–4582.
- 4 Y. Sun, Y. Cao, L. Wang, X. Mu, Q. Zhao, R. Si, X. Zhu, S. Chen, B. Zhang, D. Chen and Y. Wan, Gold catalysts containing interstitial carbon atoms boost hydrogenation activity, *Nat. Commun.*, 2020, **11**, art n:4600.
- 5 J. E. Ortiz-Castillo, R. C. Gallo-Villanueva, M. J. Madou and V. H. Perez-Gonzalez, Anisotropic gold nanoparticles: A survey of recent synthetic methodologies, *Coord. Chem. Rev.*, 2020, **425**, 213489.
- 6 F. Wang, Y. Guo, Y. Zhang and P. Tang, Silver-Catalyzed Dibromotrifluoromethoxylation of Terminal Alkynes, *ACS Catal.*, 2021, **11**, 3218–3322.
- 7 X.-Y. Dong, Z.-W. Gao, K.-F. Yang, W.-Q. Zhanga and L.-W. Xu, Nanosilver as a new generation of silver catalysts in organic transformations for efficient synthesis of fine chemicals, *Catal. Sci. Technol.*, 2015, **5**, 2554–2574.
- 8 D. Astruc, Introduction: Nanoparticles in Catalysis, *Chem. Rev.*, 2020, **120**, 461–463.
- 9 G. Kumari, R. Kamarudheen, E. Zoethout and A. Baldi, Photocatalytic Surface Restructuring in Individual Silver Nanoparticles, *ACS Catal.*, 2021, **11**, 3478–3486.
- 10 T. Ishida, T. Murayama, A. Taketoshi and M. Haruta, Importance of Size and Contact Structure of Gold Nanoparticles for the Genesis of Unique Catalytic Processes, *Chem. Rev.*, 2020, **120**, 464–525.
- 11 Y. He, J.-C. Liu, L. Luo, Y.-G. Wang, J. Zhu, Y. Du, J. Li, S. X. Mao and C. Wang, Size-dependent dynamic structures of supported gold nanoparticles in CO oxidation reaction condition, *Proc. Natl. Acad. Sci. U. S. A.*, 2018, **115**, 7700–7705.
- 12 M. Filice, M. Marciello, M. P. Morales and J. M. Palomo, Synthesis of heterogeneous enzyme–metal nanoparticle biohybrids in aqueous media and their applications in C–C bond formation and tandem catalysis, *Chem. Commun.*, 2013, **49**, 6876–6878.
- 13 R. Benavente, D. Lopez-Tejedor and J. M. Palomo, Synthesis of a superparamagnetic ultrathin FeCO<sub>3</sub> nanorods–enzyme bionanohybrid as a novel heterogeneous catalyst, *Chem. Commun.*, 2018, **54**, 6256–6259.
- 14 J. M. Palomo, Nanobiohybrids: a new concept for metal nanoparticles synthesis, *Chem. Commun.*, 2019, **55**, 9583–9589.
- 15 N. Losada-Garcia, A. Jimenez-Alesanco, A. Velázquez-Campoy, O. Abian and J. M. Palomo, Enzyme/Nanocopper Hybrid Nanozymes: Modulating Enzyme-like Activity by the Protein Structure for Biosensing and Tumor Catalytic Therapy, *ACS Appl. Mater. Interfaces*, 2021, **13**, 5111–5124.
- 16 N. Losada-Garcia, A. Rodriguez-Otero and J. M. Palomo, Tailorable synthesis of heterogeneous enzyme–copper nanobiohybrids and their application in the selective oxidation of benzene to phenol, *Catal. Sci. Technol.*, 2020, **10**, 196–206.
- 17 R. Benavente, D. Lopez-Tejedor, M. P. Morales, C. Perez-Rizquez and J. M. Palomo, The enzyme-induced formation of iron hybrid nanostructures with different morphologies, *Nanoscale*, 2020, **12**, 12917–12927.
- 18 J. Jaramillo, I. Rodriguez-Oliva, O. Abian and J. M. Palomo, Specific chemical incorporation of L-DOPA and functionalized L-DOPA-hyaluronic acid in *Candida antarctica* lipase: creating potential mussel-inspired, *SN Appl. Sci.*, 2020, **2**, art n: 1731.
- 19 J. M. Bolivar, J. Rocha-Martin, C. Mateo, F. Cava, J. Berenguer, R. Fernandez-Lafuente and J. M. Guisan, Coating of Soluble and Immobilized Enzymes with Ionic Polymers: Full Stabilization of the Quaternary Structure of Multimeric Enzymes, *Biomacromolecules*, 2009, **10**, 742–747.
- 20 C. Perez-Rizquez, D. Lopez-Tejedor, L. Plaza-Vinuesa, B. de las Rivas, R. Muñoz, J. Cumella and J. M. Palomo, Chemical Modification of Novel Glycosidases from *Lactobacillus plantarum* Using Hyaluronic Acid: Effects on High Specificity against 6-Phosphate Glucopyranoside, *Coatings*, 2019, **9**, 311.
- 21 A. D. Pagar, M. D. Patil, D. T. Flood, T. Hyeon Yoo, P. E. Dawson and H. Yun, Recent Advances in Biocatalysis with Chemical Modification and Expanded Amino Acid Alphabet, *Chem. Rev.*, 2021, **121**, 6173–6245.
- 22 J. M. Naapuri, G. A. Åberg, J. M. Palomo and J. Deska, Arylative Allenol Cyclization via Sequential One-pot Enzyme & Palladium Catalysis, *ChemCatChem*, 2021, **13**, 763–769.
- 23 M. Filice, N. Losada-Garcia, C. Perez-Rizquez, M. Marciello, M. P. Morales and J. M. Palomo, Palladium-Nanoparticles BioHybrids in Applied Chemistry, *Appl. Nano*, 2021, **2**, 1–13.
- 24 Y. Wang, H. Lu and P.-F. Xu, Asymmetric Catalytic Cascade Reactions for Constructing Diverse Scaffolds and Complex Molecules, *Acc. Chem. Res.*, 2015, **48**, 1832–1844.
- 25 Y.-C. Liu, C. Merten and J. Deska, Enantioconvergent Biocatalytic Redox Isomerization, *Angew. Chem., Int. Ed.*, 2018, **57**, 12151–12156.
- 26 F. Blume, Y.-C. Liu, D. Thiel and J. Deska, Chemoenzymatic Total Synthesis of (+)- & (–)-cis-Osmundalactone, *J. Mol. Catal. B: Enzym.*, 2016, **134**, 280–284.
- 27 S. Yu and S. Ma, Allenes in Catalytic Asymmetric Synthesis and Natural Product Syntheses, *Angew. Chem., Int. Ed.*, 2012, **51**, 3074–3112.
- 28 J. M. Alonso and P. Almendros, Deciphering the Chameleonic Chemistry of Allenols: Breaking the Taboo of a Onetime Esoteric Functionality, *Chem. Rev.*, 2021, **121**, 4193–4252.
- 29 J. Naapuri, J. D. Rolfes, J. Keil, C. Manzuna Sapu and J. Deska, Enzymatic halocyclization of allenic alcohols and





- carboxylates: a biocatalytic entry to functionalized O-heterocycles, *Green Chem.*, 2017, **19**, 447–452.
- 30 A. Fürstner, E. Kattnig and O. Lepage, Total Syntheses of Amphidinolide X and Y, *J. Am. Chem. Soc.*, 2006, **128**, 9194.
  - 31 F. Volz and N. Krause, Golden opportunities in natural product synthesis: first total synthesis of (–)-isocyclo capitelline and (–)-isochrysotricine by gold-catalyzed allene cycloisomerization, *Org. Biomol. Chem.*, 2007, **5**, 1519.
  - 32 C. Manzana Sapu and J. Deska, Chemoenzymatic total synthesis of hyperiones A and B, *Org. Biomol. Chem.*, 2013, **11**, 1376–1382.
  - 33 M. Asikainen and N. Krause, Tandem Enzyme/Gold-Catalysis: From Racemic  $\alpha$ -Allenic Acetates to Enantiomerically Enriched 2,5-Dihydrofurans in One Pot, *Adv. Synth. Catal.*, 2009, **351**, 2305–2309.
  - 34 O. Romero, B. de las Rivas, D. Lopez-Tejedor and J. M. Palomo, Effect of Site-Specific Peptide-Tag Labeling on the Biocatalytic Properties of Thermoalkalophilic Lipase from *Geobacillus thermocatenulatus*, *ChemBioChem*, 2018, **19**, 369–378.
  - 35 O. Romero, C. W. Rivero, J. M. Guisan and J. M. Palomo, Novel enzyme-polymer conjugates for biotechnological applications, *PeerJ*, 2013, e27.
  - 36 C. Godoy, B. de las Rivas, M. Filice, G. Fernández-Lorente, J. M. Guisan and J. M. Palomo, Enhanced activity of an immobilized lipase promoted by site-directed chemical modification with polymers, *Process Biochem.*, 2010, **45**, 534–541.
  - 37 M. L. Gutarra, O. Romero, O. Abian, F. A. G. Torres, D. M. G. Freire, A. M. Castro, J. M. Guisan and J. M. Palomo, Enzyme surface glycosylation on the solid phase: improve activity and selectivity of *Candida antarctica* lipase B, *ChemCatChem*, 2011, **3**, 1902–1910.
  - 38 Y. Meng, A sustainable approach to fabricating ag nanoparticles/PVA hybrid nanofiber and its catalytic activity, *Nanomaterials*, 2015, **5**, 1124–1135.
  - 39 J. M. Palomo, M. Fuentes, G. Fernández-Lorente, C. Mateo, J. M. Guisan and R. Fernández-Lafuente, General Trend of Lipase to Self-Assemble Giving Bimolecular Aggregates Greatly Modifies the Enzyme Functionality, *Biomacromolecules*, 2003, **4**(1), 1–6.
  - 40 S. Moreno-Pérez, N. Ghattas, M. Filice, J. M. Guisan and G. Fernandez-Lorente, Dramatic hyperactivation of lipase of *Thermomyces lanuginosa* by a cationic surfactant: Fixation of the hyperactivated form by adsorption on sulfo-propyl-sepharose, *J. Mol. Catal. B: Enzym.*, 2015, **122**, 199–203.
  - 41 A. A. Buglak, R. R. Ramazanov and A. I. Kononov, Silver cluster-amino acid interactions: a quantum-chemical study, *Amino Acids*, 2019, **51**, 855–864.
  - 42 A. A. Buglak and A. I. Kononov, Comparative study of gold and silver interactions with amino acids and nucleobases, *RSC Adv.*, 2020, **10**, 34149–34160.
  - 43 X.-D. Hu, B.-Q. Shan, R. Tao, T.-Q. Yang and K. Zhang, Interfacial Hydroxyl Promotes the Reduction of 4-Nitrophenol by Ag-based Catalysts Confined in Dendritic Mesoporous Silica Nanospheres, *J. Phys. Chem. C*, 2021, **125**, 2446–2453.

